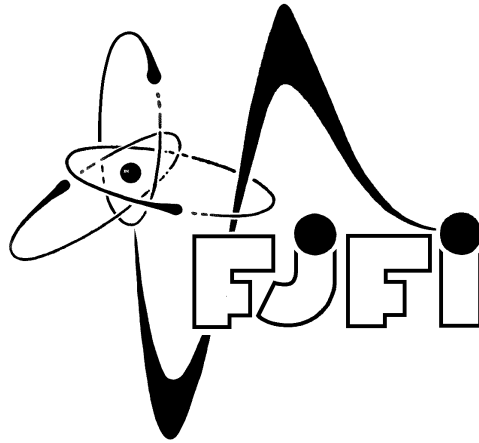


CZECH TECHNICAL UNIVERSITY IN PRAGUE
Faculty of Nuclear Sciences and Physical Engineering



Conceptual Design Report

Spark chamber

PPRA collaboration
class of 2015/2016

PPRA collaboration

Project coordinator

Matouš Vozák

Spokesperson

Zbyněk Nguyen

External construction

Hana Hruběšová

Miroslav Šaur

Internal construction

Jakub Kvapil

Ota Zaplatílek

Fill gas

Alena Harlenderová

Martin Kocmánek

Trigger and scintillators

Michal Kocan

Matouš Vozák

Theory and simulations

Filip Nechanský

Zbyněk Nguyen

Power supply

Jan Vaněk

Contents

Introduction	1
1 Cosmic radiation	2
1.1 Cosmic radiation types	2
1.1.1 Primary cosmic rays	2
1.1.2 Secondary cosmic rays	2
1.2 Muon flux	3
2 Fill gas	4
2.1 Breakdown in gas	4
2.1.1 Paschen's law	4
2.2 Choice of fill gas	5
2.2.1 Spark colour	5
2.3 Pressure of gas	5
2.4 Gas injection	6
3 Construction	7
3.1 External construction	7
3.1.1 Proposed designs	7
3.1.2 Final design	7
3.2 Internal construction	8
3.2.1 Material of electrodes	8
3.2.2 Plate deformations	9
4 Trigger	10
4.1 Scintillator	11
4.1.1 Energy deposition in the scintillator	11
4.1.2 Trigger acceptance	12
4.2 Lightguide	13
4.2.1 Lightguide simulation	13
4.3 Photomultiplier	14
4.3.1 Photomultiplier pulse	15
4.4 Discriminator and coincidence unit	15
5 Power supply	16
5.1 Transformer	16
5.1.1 Parameters to be measured	17
5.2 Clearing voltage	17
Bibliography	18

Introduction

Aim of this text is to summarize the concept of the Spark chamber project, its physics principles and the proposed design, as well as to give an outline of the expected performance.

Each second, the surface of the Earth is bombarded with various high-energy particles from outer space. In ideal case, the Spark chamber project should be able to detect the decay products of these particles, namely muons, and visualize their paths through sparks.

The text is structured as follows. In the first chapter, some facts about cosmic radiation are presented. The second chapter is focused on the gas used as the chamber fill. In the third chapter, external and internal construction is characterized. The fourth chapter is dedicated to trigger description, simulations and performance. In the last chapter, the power supply for the spark chamber is introduced.

Chapter 1

Cosmic radiation

1.1 Cosmic radiation types

High energy radiation from outer space is referred to as cosmic radiation, or cosmic rays¹. It mainly consists of stable charged particles and atomic nuclei produced in astrophysical processes. The exact origin of these particles remains a mystery, but it is thought to be mostly from stars and supernovae.

1.1.1 Primary cosmic rays

Upon reaching the top of Earth's atmosphere, the cosmic radiation is called the primary cosmic radiation. These are the particles that are produced in outer space, and thus the main component of primary cosmic rays are abundant elements in space, protons and alpha particles. The rest is composed of heavier atomic nuclei that are produced in stellar nucleosynthesis, such as carbon, oxygen or iron. The remaining component is a small amount of antimatter in the form of antiprotons or positrons, and lighter nuclei not directly produced in stars, such as lithium, beryllium or boron.

1.1.2 Secondary cosmic rays

As the primary cosmic rays interact with the atmosphere, they produce the secondary cosmic rays. They comprise various hadron decay products, causing the so-called particle showers. Among these decay products, hadrons and mesons can be found. Charged mesons – pions π^\pm and kaons K^\pm – decay mostly into muons μ^\pm , via reactions

$$\pi^- \rightarrow \mu^- + \bar{\nu}_\mu, \quad \pi^+ \rightarrow \mu^+ + \nu_\mu, \quad K^- \rightarrow \mu^- + \bar{\nu}_\mu, \quad K^+ \rightarrow \mu^+ + \nu_\mu.$$

It is muons that are of particular interest in this project, as their rather large mass causes them to be very penetrating and capable of long distance travel all the way from higher atmosphere to the ground and beneath. For this reason, muons can be detected in lower altitudes. Their observation is a clear evidence of the cosmic rays occurrence.

¹*Rays* is a term coined by history, as it was originally thought to be purely electromagnetic radiation.

1.2 Muon flux

Another argument in favor of muons is their relatively high flux at the surface of the Earth (Fig. 1.1). Their flux is only exceeded by the neutrino flux². Particle flux for other particles is several orders of magnitude lower and thus they will represent the background for this experiment.

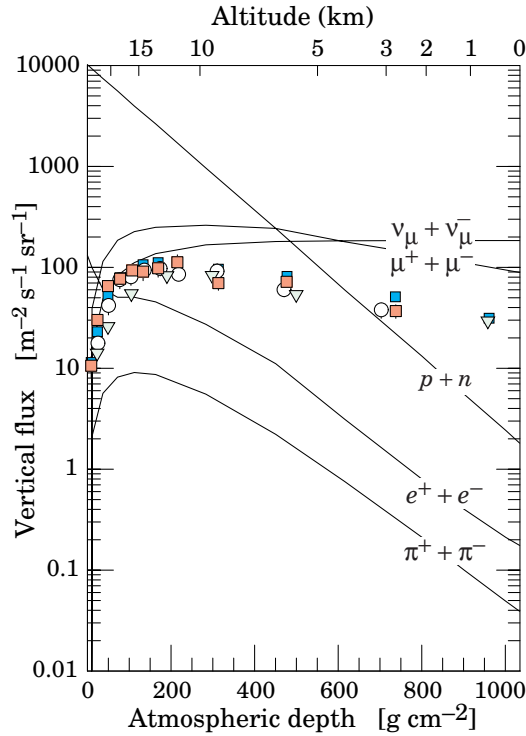


Fig. 1.1: Particle fluxes of cosmic rays with respect to atmospheric depth. The points depict measurements of μ^- with energy greater than 1 GeV. [1]

It is established that the muon flux is $70 \text{ m}^{-2} \text{ s}^{-1} \text{ sr}^{-1}$ [1], and angular distribution is proportional to $\cos \theta^{1.85}$ [1]. These properties are valid for muons with energy greater than 1 GeV and zenith angle $|\theta| < 70^\circ$. These are only rough estimates, but they are sufficient for level of precision needed. Considering these values, there will be approximately 5 muons per second passing through an area of $20 \times 20 \text{ cm}^2$.

²For their immensely high penetrating ability, neutrinos are near impossible to detect.

Chapter 2

Fill gas

One of the primary factor affecting the performance of a spark chamber is gas composition in the chamber. There are two types of fill gases used in spark chambers, noble gases and gases in which electrons are easily attached [2]. Helium, argon and neon are commonly used noble gases. Oxygen and air serve as the second type of fill gases.

2.1 Breakdown in gas

A charged particle passing through gas interacts with atoms and liberates electrons. For instance, there are approximately 30 electrons and ions created per one cm in neon [3]. When high voltage is applied between two electrodes, the following occurs: electrons and ions, generated in a gas by passing particle, are accelerated towards electrodes with opposite charge. Due to collisions, electrons may liberate other electrons; consequently, their number grows exponentially, and avalanches appear [3]. Due to recombination, some of the cations accept electrons, and turn again into neutral atoms. The recombination of the ions causes a photon radiation. These photons might create other ion pairs, leading to more avalanches. The conductive plasma channel is created when avalanches connect the anode and cathode [3], leading to electric discharge (breakdown).

Helium, neon and argon are used as fill gases because of their low electron affinity and long memory time ¹. However, presence of electronegative impurities such as oxygen can rapidly decrease the memory time [2].

In the second type of fill gases, the electrons are also liberated by charged passing particle, however they are immediately captured by high atoms with high electro-negativity such as oxygen [2]. Ions are created and if the high voltage is applied, a process analogous to previous example occurs.

2.1.1 Paschen's law

An important property of gases is the voltage at which the breakdown occurs, called the breakdown voltage. It is given by the Paschen's law

$$V = \frac{Bpd}{\ln(Apd) - \ln\left(\ln\left(1 + \frac{1}{\gamma}\right)\right)}, \quad (2.1)$$

where p is the pressure in Pascals, d is the gap distance in meters, γ is the coefficient connected to the secondary electron emission from the cathode and A , B are roughly constant for one gas at restricted E/p [7]. E is intensity of electric field.

It is necessary to say that the Paschen's law does not consider ionization of gas, therefore it estimates only the upper limit of voltage. To avoid spontaneous electric discharge, the

¹The maximal time between the passage of particle and application of high voltage.

voltage needs to be reduced below the breakdown limit. However, it is needed to be rather close to the Paschen's curve, otherwise the avalanche would not be created. The presence of free electrons liberated by traversing charged particle causes only small decrease of the breakdown voltage of gas.

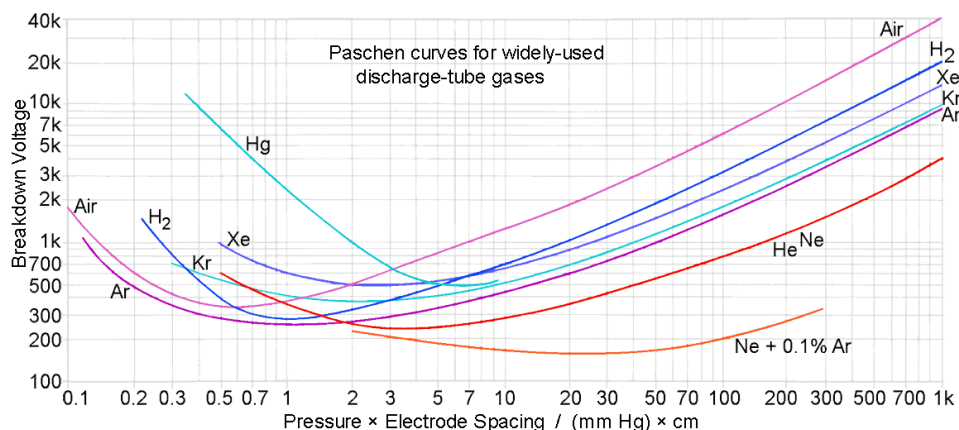


Fig. 2.1: Paschen's law [6].

The Paschen's curves for various gases can be seen in the Fig. 2.1. As evident, neon with low percentage of argon or neon with helium have sufficient characteristics, whereas air requires higher voltage than noble gases for more than two torr · cm. The dielectric strength of air at atmospheric pressure is 30 kV/cm [10]. The dielectric strengths relative to nitrogen of air, helium, neon and argon are respectively 0.97 [21], 0.15 [8], 0.16 [9] and 0.18 [8]. Therefore, the dielectric strengths of helium, neon and argon are respectively 4.7 [8], 4.9 [9], and 5.6 [8] kV/cm.

2.2 Choice of fill gas

One of the most common fill gases for spark chamber with good properties is a mixture of two noble gases: neon (70%) and helium (30%) due to a very low breakdown voltage and bright red color of a spark. Eventually, helium was chosen as the fill gas for its low breakdown voltage and other properties.

To improve spark chamber performance, small quantities of alcohol vapour can be added to the spark chamber gas. Alcohol absorbs ultraviolet light responsible for spurious sparking and acts as a quenching agent [3]. However, this improvement is insignificant for the desired purpose.

2.2.1 Spark colour

Every gas has its own colour of discharge. The colour of discharges in high purity helium, neon, argon, krypton and xenon in vacuum can be seen in the Fig. 2.2. Discharge in helium is pink-purple coloured, in neon red coloured, and in argon violet coloured. Air discharge is blue-purple-violet coloured [5].

2.3 Pressure of gas

Operating pressure of gas in the chamber will be approximately equal to atmospheric pressure 1 atm. As evident from Fig. 2.1, lower gas pressure requires lower maximum voltage. In this case, the choice of gas is not limited (even air would be a viable option). However, to



Fig. 2.2: Discharge in high purity (99.999%) helium, neon, argon, krypton and xenon in vacuum. [4]

reach low pressure, vacuum pumps are required, as well as a chamber to withstand vacuum pressure.

2.4 Gas injection

A possible approach to fill the chamber with desired gas is to drive out the air out of the chamber, causing the internal pressure to decrease. However, the chamber is not designed to withstand low pressures. Therefore, the pressure of the chamber should not be too low.

The final design employs two valves on the opposite sides of the chamber. The first valve is utilized to pump out the mixture of air and helium whereas the other to inject the desired fill gas to the chamber.

Unfortunately, the chamber will always contain a fixed finite amount of air, assuming no leak. That is unsuitable – as the breakdown voltage of air is 30 kV at 1 atm, a specific amount of air concentration might cause early quenching of sparks. Another factor influencing the purity of gas might be the helium diffusion through the chamber walls. Ultimately, this effect was concluded to be insignificant.

Chapter 3

Construction

3.1 External construction

3.1.1 Proposed designs

In the preparatory stages of construction, two options were considered. The first option was called a “bell construction – a closed experimental apparatus in a glass bell, filled with a working gas. The second option, chosen eventually as the final structure, is a “pyramid structure”.

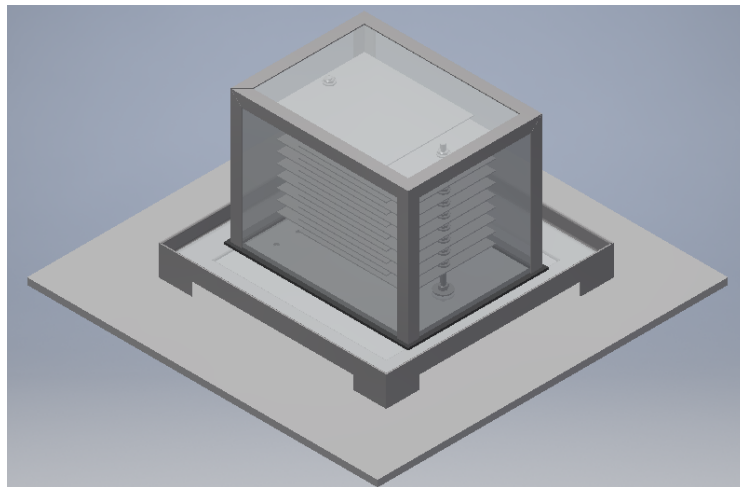


Fig. 3.1: Render of the spark chamber, isometric view. [11]

3.1.2 Final design

The final design is a tiered structure represented on Fig. 3.1. The height of the structure is assumed to be 40 cm, width and length 60 cm. The main construction materials were chosen to be polymethyl methacrylate (PMMA, also known by the trade name “plexiglass”) for the main structure, and possibly iron or wood for the mounting desk.

The main element is the chamber itself – a hollow block with a missing base. This block will be made of PMMA with dimensions of $40 \times 30 \times 25 \text{ cm}^3$ (depth x length x height) and it will be placed on a PMMA plate with dimensions of $50 \times 50 \text{ cm}^2$. The seal between the block and the plate is yet to be resolved. Three holes will be drilled in the plate. Two for the gas (for inlet and outlet), the third for the wiring. The plate itself will stand on four legs on the mounting desk. The remaining space will be used for equipment.

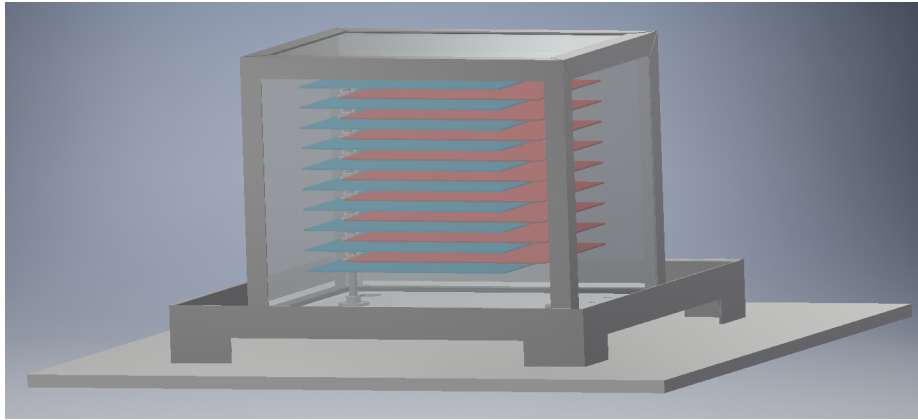


Fig. 3.2: Render of the spark chamber with inner electrodes highlighted. Colours represent electrodes of same polarity. [11]

The mounting desk will secure the main elements of the apparatus. The size is preliminarily calculated as $60 \times 60 \text{ cm}^2$, width will be chosen to ensure rigidity and stability.

3.2 Internal construction

In the main chamber volume (the PMMA box), there will be 20 plates with dimensions of $21 \times 25 \times 0.1 \text{ cm}^3$. These plates will be made of either aluminum or fiberglass (see 3.2.1). High voltage will be brought to the plates via threaded rods (2 in total for both polarities) which will be embedded to the lower PMMA plate. Using nuts, half of the plates will be mounted on one threaded rod and the rest of the plates to the other in a way that each two adjacent plates will have opposite polarity (Fig. 3.2) and their mutual distance will be 1 cm (Fig. 3.3).

To reduce the leakage current, the plates will not be fully overlapped. Instead, the active detection area will be only $20 \times 20 \text{ cm}^2$. The distance between the rod and the detection area, as well as the distance between the rod and the edge of plate, will be 2 cm. With 1 cm diameter of the rod, this gives the total length of the plate. The other precautions for avoiding the leakage current will be 0.5 cm rubber insulation on the edges of each plate.

3.2.1 Material of electrodes

As the material for plates, aluminum and copper were considered as both have lower weight, compared to other metals. Aluminum is affected by oxidation, and thus a thin layer of aluminum trioxide is created on the aluminum surface. This layer is a good insulator with resistivity of $\sim 10^{15} \Omega \cdot \text{cm}$, and it can negatively affect discharges between plates. Nevertheless, as certain amount of air will be replaced by helium, the oxidation will be significantly slower.

The other alternative for plate material is copper because of its durability. In case of copper, it is possible to use printed circuit board (PCB) that are designed for electronics. They are composed of two thin layers of copper deposited on both sides of a durable polymer.

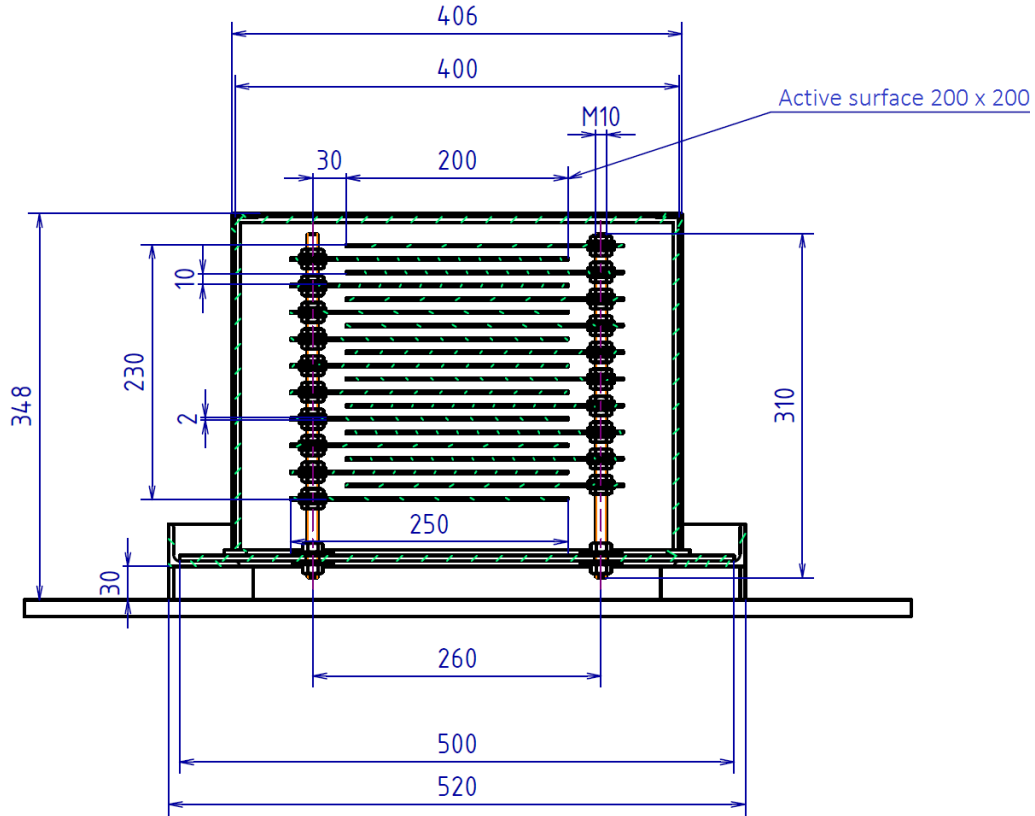


Fig. 3.3: Scheme of the spark chamber, lateral view. All dimensions are in millimeters. [11]

3.2.2 Plate deformations

Electrodes create a simple capacitor. Once the capacitor is charged, electrodes are mutually attracted. Bending leads to lessening the distance between electrodes, thus lowering the breakdown voltage, and to unwanted discharge without previous ionization.

The force between two planar electrodes is given by

$$F = \frac{1}{2} \varepsilon \frac{U^2}{l^2} S, \quad (3.1)$$

where ε is the permittivity of medium, U voltage on the electrodes, l distance between electrodes and S electrode area [12]. Plugging in the surface of approximately 10 cm^2 , voltage of 30 kV and distance of 1 cm, the force is calculated to be approximately 300 N. Therefore, if the weight of electrode is 100 g, the weight is increased by almost 30 %. However, in this configuration, only the top and bottom plates will be affected by deformation. The forces acting upon the others will cancel out.

Chapter 4

Trigger

It is possible to have electrodes charged all the time during measurement. However, it is ineffective and it can affect the measurement through spurious sparks from the mutual background. Consequently, voltage is applied on electrodes only when a trigger “fires” (a particle is detected).

The trigger is, in general, a combination of hardware and software. In this particular experiment, the trigger represents two scintillators, two lightguides, two photomultipliers, two discriminators and a coincidence unit (Fig. 4.1).

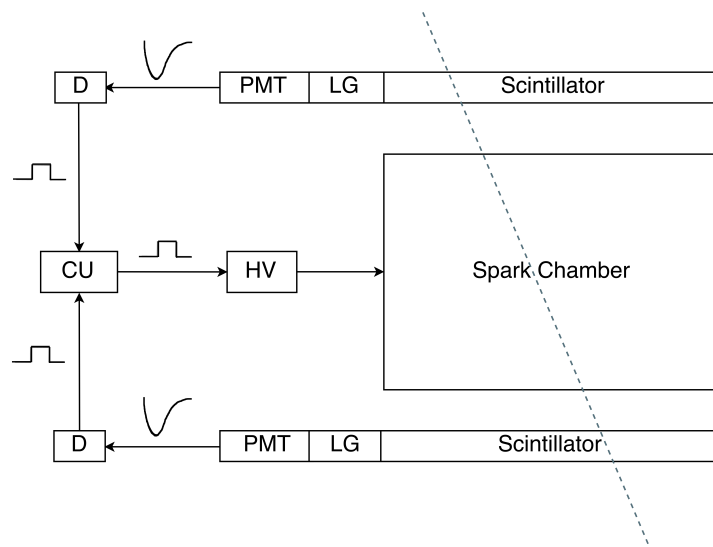


Fig. 4.1: Trigger circuit. LG = Lightguide, PMT = Photomultiplier tube, D = Discriminator, CU = Coincidence unit, HV = High voltage supply. Dashed line represents the muon trajectory.

The reason to have two circuit branches is to detect particles in coincidence. In other words, a particle is detected twice on the path given by two scintillators (the first and the second) separated by a certain distance, and the detection happens within a certain time range. This way, sparks caused by low penetrating particles (such as electrons) are filtered out as these particles do not reach both scintillators. In accordance, this experiment is focused on measuring muons, as stated in section 1.1.2.

4.1 Scintillator

When particles travel through scintillator, they lose energy, which is deposited in the atoms and molecules of the scintillator. These atoms then reach higher energy levels (excitation). They are returned to the ground state (deexcitation) by emission of visible light (scintillation), which can be detected, for instance, by a photomultiplier.

Scintillators can be made of organic or inorganic materials. The chosen scintillator is an organic scintillator manufactured by Nuvia [14] with characteristics in Tab. 4.1.

Density	1.03 g/cm ³
Index of refraction	1.57
Softening point	70-75°
Luminous flux (power)	65° (in comp. with anthracen)
Afterglow duration	2.5 ns
Maximal wavelength	420-440 nm

Tab. 4.1: Characteristics of the scintillator. [15]

The layer of a silicon gel was applied on the surface of prepared scintillator. A lightguide (section 4.2) was added on one side of the scintillator and the rest was covered by aluminum foil for better refraction of light on the surface. The resulting block was wrapped with a black tape.

4.1.1 Energy deposition in the scintillator

Simulation of transition of the muon through the scintillator was done using Monte Carlo simulator Geant 4 [17]. Two scintillators of different widths (1 cm and 2 cm) were studied, for muons with energy ranging from 1 GeV up to 200 GeV. The muon flux is taken from the section 1.2. Since the flux falls approximately as $E^{-2.7}$ [1], higher energies than 200 GeV form negligible part of the spectrum. Therefore, it is not necessary to study these.

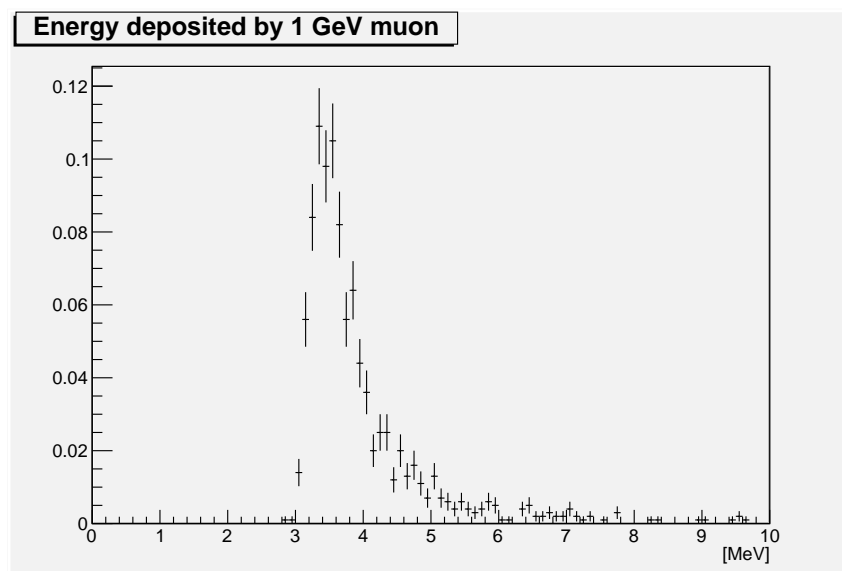


Fig. 4.2: Spectrum of energy deposited in 2 cm thick scintillator by 1 GeV muon.

The simulation was repeated 1000 times for each tested energy and showed that muon deposits approximately the same amount of energy across the whole energy spectrum. For 1 cm it is about 2 MeV, whereas for 2 cm scintillator it is 4 MeV. This suggests linear dependency typical for thin absorbers. Example of energy deposition spectrum for 1 GeV muon is in Fig. 4.2.

Since total energy will not be measured, energy resolution is not important. However, a minimal deposited energy is needed in order to detect the signal. The 2 cm were deemed to be satisfactory, as confirmed later by preliminary tests of the scintillator.

4.1.2 Trigger acceptance

In order to determine the percentage of muons, which will pass through both scintillators, a simulation created in ROOT [18] was used. It simulated muons with random direction based on angular distribution at the first scintillator and then determined whether such muons pass through the second one. Due to the nearly cube shape of the chamber, muons from zenith angle greater than $\approx 45^\circ$ will not be measured.

Simulation was compared to results of measurement [19] to determine whether it produces at least qualitatively similar results. Our simulation for the configuration predicted 78.7 counts/min, while the measurement yielded 77 counts/min, a difference smaller than 2 %.

Final version of the trigger system consists of two scintillators with area $20 \times 20 \text{ cm}^2$ separated by 25 cm. This should yield around 2.27 muons per second. Efficiency is around 40 % and its dependence on position is in Fig. 4.3. Since other not yet known factors (such as trigger efficiency or dead time) will reduce the final number of muons, it is impossible to determine the exact number. Efficiency of other spark chambers¹ can be estimated to be around 10-20 %, providing about one muon every two to five seconds.

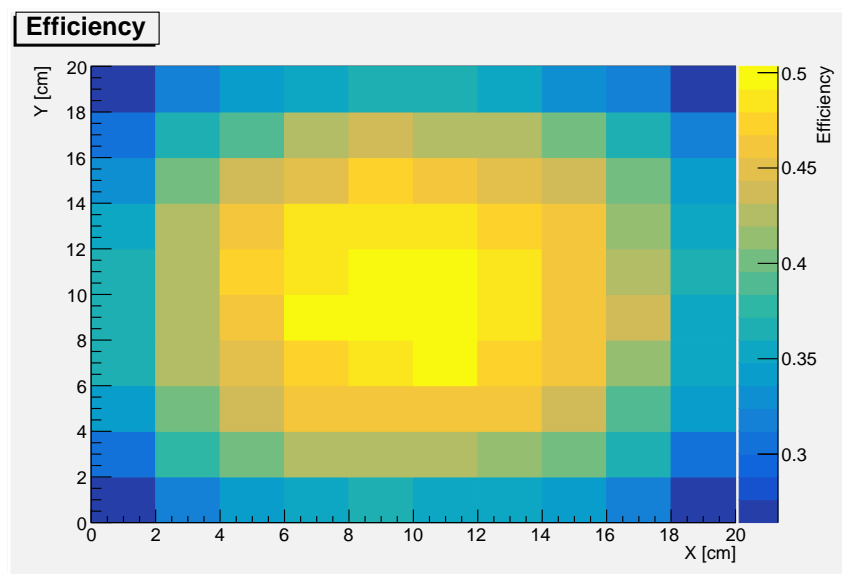


Fig. 4.3: Fraction of muons which will pass through both scintillators based on their position on first scintillator.

¹Which was roughly estimated using the simulation and frequency of events.

4.2 Lightguide

Since the scintillator is 20 cm wide while the photomultiplier only 5 cm wide, best way to connect these two components had to be decided.

Lightguide is made of glass or plastic material transparent to scintillation light, shaped in a way best suited to guide the light to the photomultiplier. It uses total reflection and reflective material to maximize efficiency, and in some cases, it can be quite complicatedly shaped.

A simple wedge was used as the lightguide. To optimize its length, a simulation was prepared. It was rewritten from simulation used in [20] and as in previous case done in ROOT [18]. It used simplified 2D model of the situation which was considered to be sufficient.

4.2.1 Lightguide simulation

First, position of the incident particle is generated. Then, certain number of photons with random direction is produced and their trajectory is computed until the photon is either absorbed or reaches the photomultiplier.

In the simulation from [20], photon was absorbed when it traveled more than 100 cm. For this project, other possibilities were considered, e.g. random absorption on walls or dependence on whether the reflection is total or not. Eventually, only requirement on incident angle of photons at the photomultiplier was added. Also, smearing of reflection angle was implemented to simulate unevenness of the surface.

Results clearly showed that the shorter the lightguide, the better the efficiency, and that this applies even for any combination of conditions on photons mentioned earlier. A length of 5 cm with entry window 20 cm wide and photomultiplier window 5 cm wide was chosen.

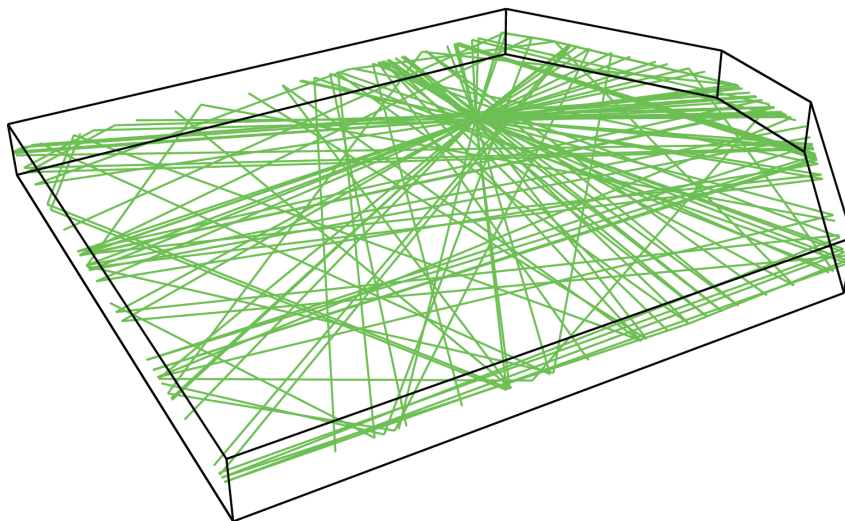


Fig. 4.4: Photon propagation through the scintillator for one particle emitting 100 photons.

An example of an event with 100 photons is showed in Fig. 4.4. Efficiency, or percentage of photons which arrive at the photomultiplier, is plotted in Fig. 4.5. The biggest efficiency is near the lightguide, the lowest at the center of the two longer edges.

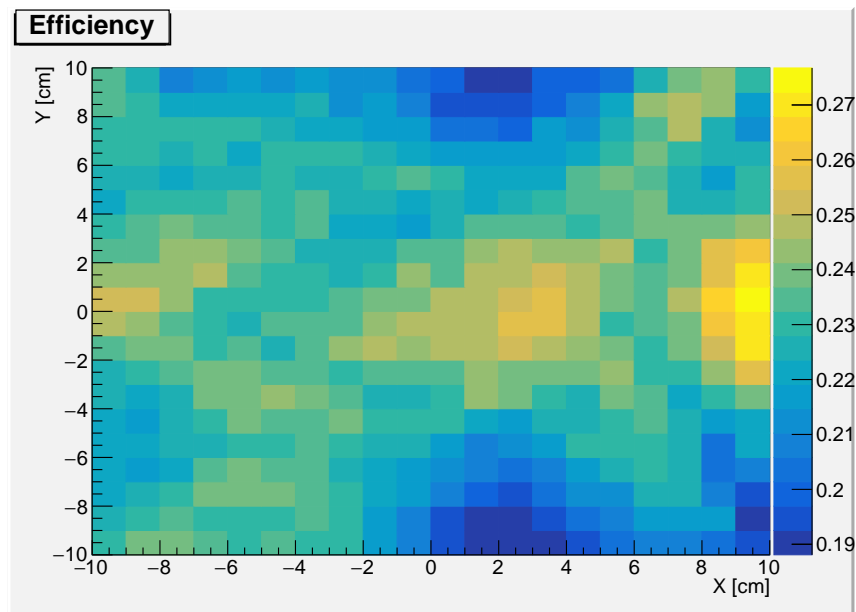


Fig. 4.5: Fraction of emitted photons which reach the photomultiplier, based on position of muon on scintillator, where the lightguide and photomultiplier are on right side of the scintillator.

4.3 Photomultiplier

It is important to convert the light signal from the scintillator to an electric signal. Photomultiplier is a device, in which the light is converted into electrons due to a photo-effect on a photocathode. Unfortunately, the number of created electrons is too low. Therefore, electrons, created on photocathode, are pulled towards set of anodes, where more electrodes are created due to secondary emission. All electrons are collected on the last electrode, representing the signal. The characteristic of the photomultiplier used for the project can be found at [22].

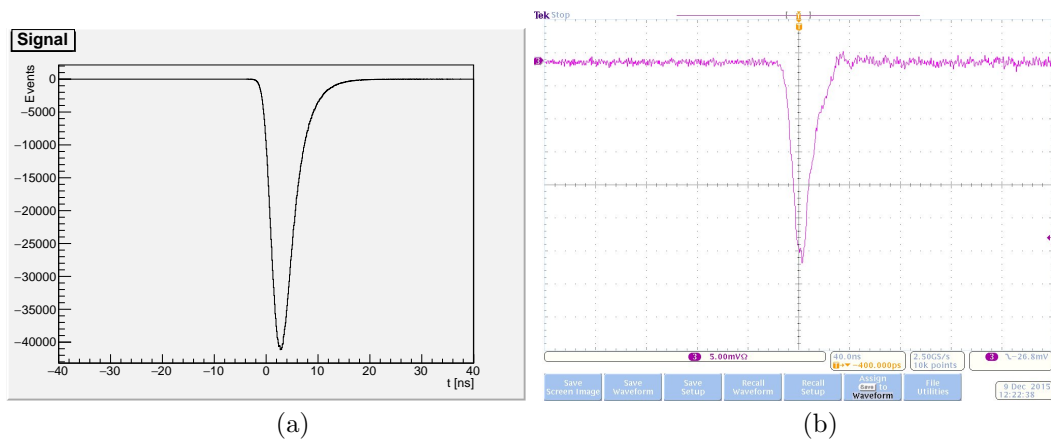


Fig. 4.6: (a) Simulated dependence of current on time. (b) Measured dependence of current on time

4.3.1 Photomultiplier pulse

Since the scintillator has a delay time of cca 2.5 ns^2 (Tab. 4.1), time of arrival derived from the trajectory length was smeared by a random value of exponential distribution. Finally, other various effects (such as electronic read-out) were simulated as Gaussian with $\sigma \approx 2$. In Fig. 4.6, there is a comparison of the simulated time progress and the measured one.

Aside from quicker decay in the end of the measured spectrum, simulation seems to produce quantitatively correct results. Variables as decay time or parameters of the Gaussian smearing will be better estimated using the data.

4.4 Discriminator and coincidence unit

To detect the signal from photomultiplier by a coincidence unit, the signal has to be rectangular. Solution is to use a discriminator with an amplifier to modify a signal to the required shape and height. As the incoming signal has not been fully studied, the type of discriminator is still in question. However, the coincidence unit will be most likely a **Beaglebone black** [16]. If the signal from both scintillators is in coincidence, it will be sent to the high voltage supply which provides the charge for the electrodes.

²The real value could be determined from measurement in the future.

Chapter 5

Power supply

One of the key elements of a spark chamber is a power supply. A high voltage (HV) and a low voltage (LV) supply will be required. As mentioned in chapter 4, the HV will be applied only when the trigger fires. The delay between the muon detection in the trigger and switching on the HV supply must be lesser than $\approx 0.1 \mu\text{s}$. If the HV supply is switched on any later, the electron-ion pairs created by the passing muon recombine and the signal will be lost, in other words, there will be no spark discharge.

Next aspect of the HV supply is the magnitude of the voltage. From the design in question it is assumed that the required voltage is between 7 – 10 kV. Therefore, the main characteristic is the ability to provide relatively high voltage in a very short time.

5.1 Transformer

The proposed HV supply is a transformer shown in Fig. 5.1. Exact parameters are yet to be measured.

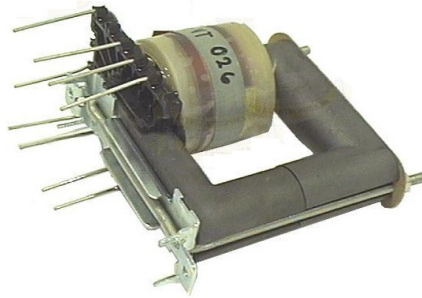


Fig. 5.1: Transformer to be used as HV supply.

From what is currently known, the transformer should deliver approximately 4 kV pulse at the output (secondary coil) from cca. 10 V pulse at the input (primary coil). One transformer is thus not enough for the desired voltage, whereas two should meet the requirements. One way of connecting these two transformers into the electrical circuit of the spark chamber is the following: one transformer connected to one set of plates of the spark chamber, the second one to the remaining plates.

The transformers will be set in parallel configuration as shown in Fig. 5.2. The LV pulse from the coincidence unit will be delivered to the primary coils of the transformers at the same time, which will generate two simultaneous HV pulses at the output. These HV pulses will have opposite magnitudes as one of the primary coils (or alternatively secondary coils) will be connected to the HV supply circuit with opposite polarity. As a result, a total voltage up to 8 kV can be generated between the two sets of plates.

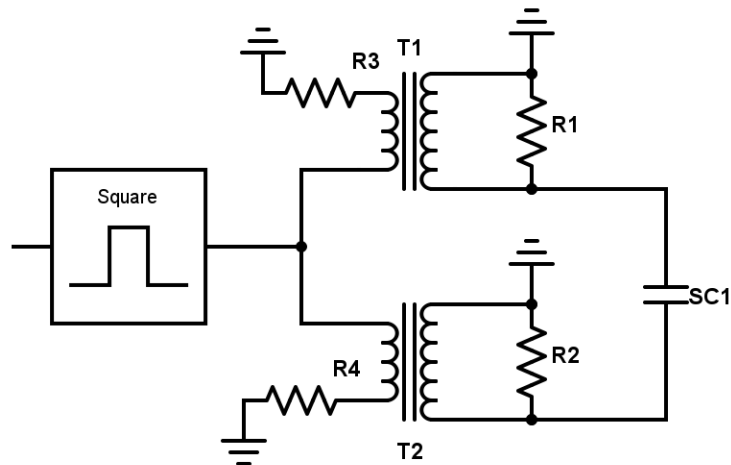


Fig. 5.2: Simplified scheme of the HV supply of the spark chamber. Square refers to LV pulse form coincidence unit; T1 and T2 are transformers; R1, R2, R3 and R4 are resistors and SC1 represents the spark chamber. Note the opposite polarities at the primary coils of the transformers.

5.1.1 Parameters to be measured

As evident from Fig. 5.1, there are several pin pairs connected to the transformer, each pair connected to one of the transformer coils. The first step is to determine which pin pairs are connected to each other and assign the individual coils to the pin pairs. The second step is to find out the transformation ratio of the primary coils. These measurements will yield all the required specifications of the transformer for further design considerations.

5.2 Clearing voltage

Clearing voltage is a low voltage applied to the plates of the spark chamber, collecting remaining ions after the spark discharge is quenched. Such precaution prevents recombination of electrons created by the most recent ionization and ions originating from previous ionizations.

Two things have to be resolved. First, the connection of the LV supply into the spark chamber electrical circuit, or more specifically, its protection from the HV pulses generated by the HV supply. The proposition is to connect the LV and HV supply in a series circuit. Second, the voltage delivered by the LV supply. There are no definite numbers yet, but the voltage will most likely be ≈ 100 V.

Bibliography

- [1] K.A. OLIVE ET AL., *Review of Particle Physics – Cosmic Rays*, Chin. Phys. C, **38**, 090001, (2014) and 2015 update, [accessed 1/2016] <http://pdg.lbl.gov/2015/reviews/rpp2014-rev-cosmic-rays.pdf>
- [2] S. MIYAMOTO, *Discharge Chamber.*, Il Nuovo Cimento, Volume 27, Issue 6, pp 1325-1346, (1963)
- [3] J. COLLINS, *Construction of a Prototype Spark Chamber*, (2010), arXiv:1010.4010
- [4] EBAY, *Set of noble gases in ampules – He Ne Ar Kr Xe discharge lamps*, [accessed 12.1.2016], <http://www.ebay.com/itm/Set-of-noble-gases-in-ampoules-Helium-Neon-Argon-Krypton-Xenon-discharge-lamps-/171192525325>
- [5] WIKIPEDIA, *Ionized-air glow*, [accessed 12.1.2016], http://en.wikipedia.org/wiki/Ionized-air_glow
- [6] D. W. KNIGHT, *Gas Discharge Tubes - Introduction*, (2013), [accessed 12.1.2016], http://www.g3ynh.info/disch_tube/intro.html
- [7] WIKIPEDIA, *Paschen's law*, [accessed 12.1.2016], https://en.wikipedia.org/wiki/Paschen's_law
- [8] A.K.,VIJH, *Communication on the Relative Electric Strengths and the Molecular Weights of Gases, Electrical Insulation*, IEEE Transactions on, Volume EI-12, Issue 4, pp 313-315, (1977), DOI: 10.1109/TEI.1977.297984
- [9] A.K.,VIJH, *Electric strenght and molecular properties of gaseous dielectrics, Electrical Insulation*, IEEE Transactions on, Volume EI-17, Issue 1, pp 84-87, (1982), DOI: 10.1109/TEI.1982.
- [10] B.A.,VEDENSKY AND B.M VUL, *Encyclopedic Dictionary in Physics*, B. M. Eds, Vol. 4, Soviet Encyclopedia Publishing House, Moscow, (1965)
- [11] *Render of the spark chamber*, courtesy of Stanislav Škoda
- [12] COLLECTIVE OF AUTHORS, *Kondenzátor, mapování elektrostatického pole (Capacitor, electrostatic field mapping)*, Manual to assignment, Department of Physics, Faculty of Nuclear Sciences and Physical Engineering at the Czech Technical University, (2015), [accessed 1/2016], http://praktikum.fjfi.cvut.cz/pluginfile.php/4352/mod_resource/content/1/Kondenzator-2015-Feb-22.pdf
- [13] W.F. HANLON, *Cosmic ray spectrum*, [accessed 1/2016], <http://www.physics.utah.edu/~whanlon/spectrum.html>
- [14] NUZIA, *Official website*, [accessed 1/2016], <http://www.nuvia.cz/en>
- [15] NUZIA, *Plastic scintillators*, [accessed 1/2016], <http://146-2-13-46.tmcz.cz/index.php/en/sluzainze-en/scintilaci-materialy-en/plast-scintilator>

- [16] BEAGLEBOARD.ORG, *Beaglebone black platform*, [accessed 1/2016], <http://beagleboard.org/BLACK>
- [17] GEANT 4, *Official website*, [accessed 1/2016], <https://geant4.web.cern.ch/geant4/>
- [18] ROOT, *Official website*, [accessed 1/2016], <https://root.cern.ch/>
- [19] M. BEKTASOGLU, H. ARSLAN, *Investigation of the zenith angle dependence of cosmic-ray muons at sea level*, *Pramana*, May 2013, Volume 80, Issue 5, pp 837-846, (2013)
- [20] COLLECTIVE OF AUTHORS, *Conceptual design report, TOF detector*, (2014), [accessed 1/2016], http://physics.fjfi.cvut.cz/files/predmety/02PPRA/Docs/cdr_2014-15.pdf
- [21] W. T. ZHUGG, *Handbook of Electrical and Electric Insulating Materials*, Van Nostrand Reingold, New York, (1986)
- [22] ET ENTERPRISES, *9266B Photomultiplier specifications*, (2010), [accessed 13.1.2016], <https://my.et-enterprises.com/pdf/9266B.pdf>